EXPERIMENTAL INVESTIGATION OF WALL NUCLEATION CHARACTERISTICS IN FLOW BOILING

Caleb S. Brooks
School of Nuclear Engineering
Purdue University
West Lafayette, Indiana, 47907
csbrooks@purdue.edu

Nicolás Silin
CONICET-CNEA and Instituto Balseiro
Bariloche, Rio Negro, 8400
Argentina
silin@cab.cnea.gov.ar

Takashi Hibiki
School of Nuclear Engineering
Purdue University
West Lafayette, Indiana, 47907
hibiki@ecn.purdue.edu

Mamoru Ishii
School of Nuclear Engineering
Purdue University
West Lafayette, Indiana, 47907
ishii@purdue.edu

Wall nucleation experiments have been performed in a vertical annulus test section for investigation of the bubble departure diameter and bubble departure frequency. The experimental data in forced convective subcooled boiling flow is presented as a parametric study of the effect of wall heat flux, local bulk liquid sub-cooling, liquid flow rate, and system pressure. The data is shown to extend the database currently available in literature to a wider range of system conditions. Along with the current database in forced convective flow, the available models for bubble departure size and frequency are reviewed and compared with the existing database. The prediction of the bubble departure frequency is shown to require accurate modeling of the bubble departure diameter which has poor agreement with the experimental database.

Keywords: wall nucleation, bubble departure diameter, bubble departure frequency, subcooled boiling, annulus, heat transfer

Nomenclature

$A\ b\ C\ c\ d\ e$	constants [-]
Bo	boiling number [-]
C_B	buoyancy coefficient [-]
C_D	drag coefficient [-]
C_s	surface tension coefficient [-]
D_d	departure diameter [m]
D_p	dry patch diameter [m]
D^+	dimensionless diameter [-]
f	departure frequency [s^{-1}]
G	mass flux [$kg/(m^2 \bullet s)$]
g	gravitational constant [m/s^2]
h_c	heat transfer coefficient [$W/(m^2 \bullet K)$]
h_{fg}	latent heat of vaporization [J/kg]
$j_{f,in}$	inlet liquid velocity
Ja_{sub}	Jacob number calculated from subcooling [-]
Ja_{sup}	Jacob number calculated from superheat [-]
k	thermal conductivity [$W/(m \bullet K)$]
N_f	non-dimensional departure frequency [-]
P	pressure [Pa]
q''	heat flux [W/m^2]
R_c	cavity radius [m]
ΔT_{sub}	local bulk liquid subcooling [K]
ΔT_w	wall superheat [K]
T_i	instantaneous surface temperature [K]
t_G	growth time [s]
t_W	wait time [s]
Greek symbols	
α	thermal diffusivity [m^2/s]
ρ	density [kg/m^3]
σ	surface tension [N/m]
Φ	contact angle [rad]
Subscripts	
b	bulk
Calc	calculated value
Exp	experimental value

f	liquid
g	gas
lo	lift off
m	maximum
NB	nucleate boiling
sat	saturation
w	wall

1 Introduction

A current shortcoming in the understanding of multi-phase flows with heat transfer is the wall nucleation phenomena. Particularly in the subcooled boiling regime, the vapor phase source is largely due to the creation of small bubbles in cavities of the heated surface. Therefore predicting the wall nucleation characteristics is very important to the solution of two-phase flow field equations through the vapor and interfacial area concentration source terms, and the vapor phase boundary condition. A better understanding of wall nucleation is also necessary for a mechanistic approach to understanding boiling heat transfer and low quality critical heat flux.

Considering its importance and impact in the multi-phase flow field equations and closure relations, it is no surprise that a large number of studies have been dedicated to understanding wall nucleation. Many early studies can be found on pool boiling systems however only limited experimental data is available in forced convective boiling systems. With advancements in imaging capability coming in the past decade more studies can be found discussing the characteristics of the wall nucleation phenomenon in forced flow conditions. While the nucleation process between the pool boiling and forced flow boiling systems are similar in principle, bubble growth in a forced flow condition must occur through much steeper temperature gradients and be exposed to turbulent fluctuations in the liquid phase. For these reasons the forced flow boiling condition is considered to be of a much higher order of complexity than the pool boiling case.

The wall nucleation process is characterized by three main terms: active nucleation site density describing the number of cavities producing vapor bubbles, bubble departure diameter which characterizes the size of the vapor bubbles generated, and the bubble departure frequency giving the rate at which a bubble is produced at a nucleation site. In this work a thorough review of the current widely used bubble departure frequency and bubble departure diameter models are presented along with the current available database for benchmarking these models. From the review of the available database it is clear that the number of conditions and range of conditions is very limited. Therefore a new dataset is presented which covers a wide range of experimental conditions. From this new dataset a parametric study of the trend in departure characteristics with system and flow conditions is discussed in detail. This parametric study is important for informing the future modeling of the nucleation characterizes by highlighting the dominant influences and their affect. Lastly the existing models for departure diameter and frequency are benchmarked against the new and existing data.

The current state of the wall nucleation modeling is presented in detail along with available data from literature to be used for model benchmark. The modeling of the active nucleation site density by Hibiki and Ishii [1] is considered as the state-of-the-art and has been benchmarked by a large dataset [2]. Therefore, this study is focused on the evaluation of the bubble departure diameter and bubble departure frequency. There have been three major approaches to modeling the characteristic nucleation bubble size and departure frequency in boiling flows: energy balance approach, force balance approach, and correlation approach. These models are summarized in Tab.1.

The departure frequency can be described by the bubble wait time, t_W, and bubble growth time, t_G, simply by

$$f = \frac{1}{t_W + t_G} \tag{1}$$

where the wait time represents the time from bubble departure

Table 1. Available wall nucleation models

Bubble Departure Diameter Modeling	
Energy Balance Approach	
Unal [3]	$q''\frac{pD_b^2}{4}\left(1-\frac{D_p^2}{D_b^2}\right)=h_c D T_{sub}\frac{pD_b^2}{2}+\frac{p}{6}r_g h_{fg}\frac{dD_b^3}{dt}$
Force Balance Approach	
Fritz [4]	$D_d = 0.022f\sqrt{\frac{s}{gDr}}$
Kocamustafaogullari and Ishii [5]	$D_d = 0.0012\left(\frac{Dr}{r_g}\right)^{0.9} D_{d,Fritz}$
Harada et al. [6]	$D_d = \frac{1}{2}\left(\frac{C_s s}{C_B g(r_f - r_g)}\right)^{0.5}$
Correlation Approach	
Prodanovic et al. [7]	$D_m^+ \equiv \frac{D_m s}{r_f a_f^2} = AJa_w^b\left(\frac{T_w - T_b}{T_w - T_{sat}}\right)^c\left(\frac{r_f}{r_g}\right)^d\left(\frac{q''}{Gh_{fg}}\right)^e$
Bubble Departure Frequency Modeling	
Energy Balance Approach	
Podowski et al. [8]	$t_W = \frac{1}{2C_1}\left(-C_3+\sqrt{C_3^2-4C_1C_2}\right)^2$ $C_1 = \frac{2q''}{p}\left(\frac{k_w}{\sqrt{pa_w}}+\frac{k_f}{\sqrt{pa_f}}\right)^{-1}, C_2 = \frac{(T_i^+ - T_b)R_c}{\sqrt{pa_f}}$ $C_3 = T_i^+ - \frac{q''R_c}{p\sqrt{pa_f}}\left(\frac{k_w}{\sqrt{pa_w}}+\frac{k_f}{\sqrt{pa_f}}\right)^{-1} - \frac{2sT_{sat}}{R_c h_{fg}}\left(\frac{1}{r_g}+\frac{1}{r_f}\right)T_{sat}$ $t_G = \frac{1}{2A_1}\left(-A_3+\sqrt{A_3^2-4A_1A_2}\right)^2$ $A_1 = \frac{q''}{k_w}, A_2 = \frac{2(T_i - T_{sat})}{\sqrt{pa_w}}, A_3 = \frac{D_d r_g h_{fg}}{2k_w}$

Force Balance Approach	
Cole [9]	$f = \left[\frac{4g(r_f - r_g)}{3r_f C_D D_d}\right]^{0.5}$
Correlation Approach	
Basu et al. [10]	$t_W = 139.1 DT_w^{-4.1}$ $t_G = 0.0222 e^{(0.02Ja_{sub})} \frac{D_d^2}{a_f Ja_{\sup}}.$
Situ et al. [11]	$N_f \propto \frac{fD_d^2}{a_f} = 10.7 \left[\frac{q_{NB} D_d}{a_f r_g h_{fg}}\right]^{0.634}$
Euh et al. [12]	$N_f \propto \frac{fD_d^2}{a_f} = 1.6 \left[\frac{q_{NB} D_d}{a_f r_g h_{fg}}\right]^{1.3}$

until the next bubble is first initiated in the nucleation site cavity, and the growth time is the time from the initiation until the bubble departs the site. In forced convective boiling, the nucleating bubbles are exposed to a much higher temperature gradient of the liquid phase than in the case of pool boiling. Therefore, the wait time can be significantly different from the pool boiling case due to greater local temperature fluctuation from mixing of the departing bubbles as well as turbulent convective effects which act to lower the heating surface temperature. The growth time will also be affected by the bulk fluid motion as forces acting to remove the nucleating bubble will alter the maximum bubble size and therefore the amount of time growing on the surface.

The available data for bubble departure frequency in flow boiling systems is very limited. As shown in Tab.1, the bubble departure frequency has been modeled as a function of bubble departure diameter and shown to be a strong function of the departure size. Therefore the departure frequency database should contain bubble departure diameter as well as sufficient conditions in order to determine the necessary parameters effecting the bubble nucleation. From an extensive literature review, the three datasets of Klausner et al. [13], Basu [14], and Yuan et al. [15] have been selected for the study of the bubble departure diameter and the two datasets of Basu [14] and Okawa et al. [16] provide the required information necessary to describe the bubble departure frequency phenomena. A summary of the datasets is given in Tab. 2. In the study of Okawa et al. [16] the growth time represents the time from the onset of vapor growth until bubble lift-off. Some error and differences to the present dataset is expected as the bubble frequency and diameter have been defined differently. The bubble lift-off frequency and departure frequency are the same under conditions where bubbles do not condense while sliding on the heated surface. The lift-off diameter may be an adequate bubble length scale for modeling bubble departure frequency.

Table 2. Available database for model benchmark

Study	Klausner et al. [13]	Basu [14]	Okawa et al. [16]	Yuan et al. [15]	Present Study
Measurement	D_d	D_d, f	D_{lo}, f	D_d	D_d, f
Conditions	35	19	28	21	83

Orientation	Hor.	Vertical	Vertical	Vertical	Vertical
Fluid	R113	Water	Water	Water	Water
Geometry	Square	Square	Tube	Rect.	Annulus
Hydr. Diameter [mm]	25	39.2	20	3.85	19
Contact Angle [deg.]	40.5*	30	45	NA	57
Pressure [kPa]	132-213	103	120	121-1040	150, 300
Heat Flux [kW/m^2]	11-26	210-950	110-550	71-334	100-492
Mass Flux [kg/m^{2}s]	113.287	235-685	90-1500	76-603	235-986
Subcooling [^{o}C]	NA	7-46	10,20	20-36	5-40
*average of measured advanced and receding contact angles					

2 Experimental Approach

The annular test facility was designed based on geometric and thermal-hydraulic similarities of a prototypic boiling water nuclear reactor. The test facility is given in great detail by Ozar et al. [18] with only a small modification for this study to the heater rod length. An identical heater rod with a shorter heated length was used in this study to perform test at higher heat flux. The test section is shown in Fig. 1 with relevant dimensions and instrument locations. A cartridge heater with outer diameter of 19.1 mm and pipe with inner diameter of 38.1 mm form the annulus geometry. The heater rod accommodates five thermocouples, which are embedded in the heater surface and provide the surface temperature. These thermocouples are located at the same axial locations as the instrumentation ports and provided the surface temperature of the heater rod. A pre-heater and condenser are used to control and stabilize the inlet conditions. A pressurizing tank with a large gas space was used to set the system pressure and dampen any pressure fluctuations.

A bubble nucleation site is recorded with a high speed camera at z/D_h=19.6 from the start of the heated section (z/D_h=43.8 from the test section inlet). A pressure and bulk flow temperature measurement is recorded less than one hydraulic diameter downstream of the nucleation site. The high speed camera recorded 4.36 seconds at a frame rate of 10,000 fps and resolution of 128 x 256 pixels. The images were calibrated based on the apparent size of a small groove in the heater rod on the opposite side of the test section. The groove, which runs the thermocouple wire for the embedded thermocouples, was measured under a microscope to be 397±20 µm. With the same camera and lens settings used in the experiments, the groove was found to be 84±5 pixels while in the test section filled with saturated water. Therefore the calibration for the images resulted in a 4.7±0.4 µm/pixel.

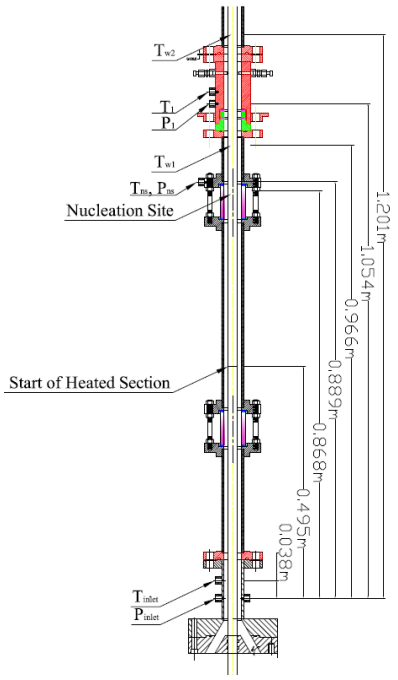

Fig. 1: Schematic of the experimental test section

The same nucleation site is measured for all conditions allowing for a parametric study of heat flux, pressure, inlet liquid velocity, and local sub-cooling. At least 100 departing bubbles were manually measured for each case to characterize the departure frequency and departure diameter. By averaging over 100 bubbles, the experimental error in departure diameter from the measurement technique is less than 2% of the measured value. The statistical accuracy of the data is more difficult to determine since a very large number of bubbles cannot be measured for each condition. This is an issue with all past datasets and is analyzed in the extension to this work [17]. The departure frequency was calculated by dividing the number of departing bubbles counted by the number of frames processed, multiplied by the cameral frame rate. The new dataset is summarized with the current database in Tab. 2 and tabulated in the Appendix.

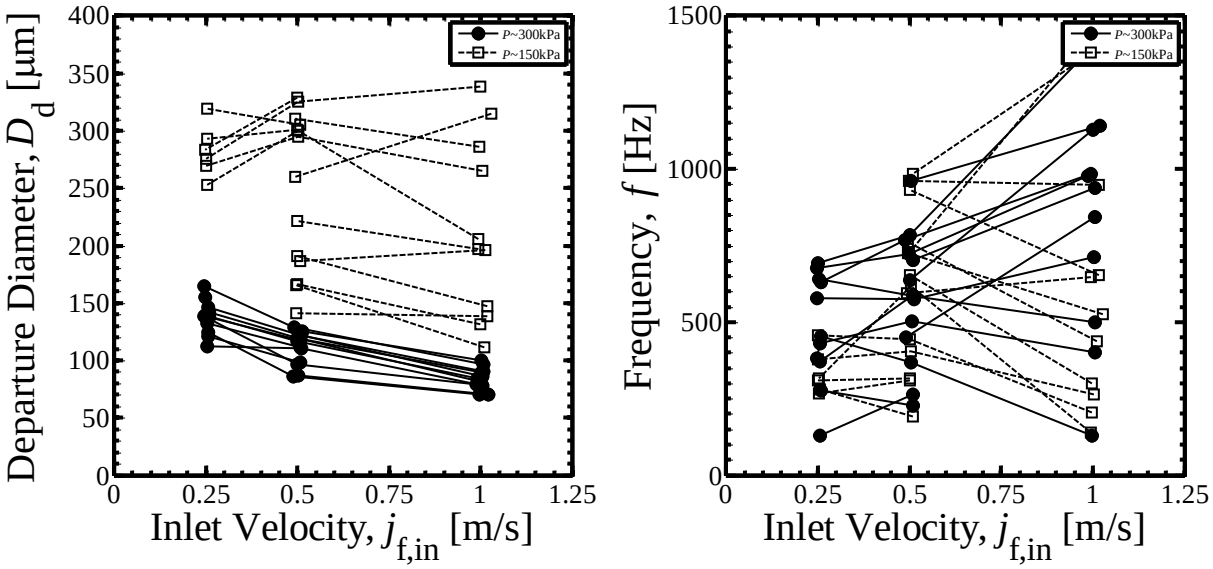

Fig. 2: Effect of liquid velocity on bubble departure diameter and frequency

3 Results and Discussion

Based on the limited database available in literature, new nucleation experiments are described in detail within this section. The new dataset highlights the dependence of the departure diameter and frequency on different system conditions. The experimental dataset is discussed in detail in this section and tabulated in Appendix A. From the complete database, consisting of the new experiments and data available in literature, the past models of departure diameter and departure frequency are evaluated to determine the current state of wall nucleation prediction capability in flow boiling.

3.1 Bubble Departure Diameter Data

The test matrix was constructed such that a parametric study of the effects of system pressure, heat flux, local bulk subcooling, and liquid inlet velocity can be thoroughly presented. The effect of system pressure on bubble departure diameter is shown by Figs. 2-4. The figures present a study of each effect by plotting the data

in groups where the other effects are held constant. Therefore each line represents constant conditions in the other degrees of freedom. Therefore the figures indicated the overall trend in the departure diameter and departure frequency for each respective parameter (i.e. velocity, subcooling, and heat flux). The slope of the lines collectively show the dependence of the data on the parameter of interest. Also in each figure the open square makers and closed circle markers represent the low and elevated pressure conditions respectively. The departure diameter is found to decrease with increasing pressure. This decreasing trend with increase pressure is largest at low bulk liquid subcooling and wall heat flux where the departure diameter may be reduced by as much as two thirds by doubling the system pressure and holding the other system conditions constant. At high liquid subcooling conditions shown in Fig. 3 the pressure effect is less significant which suggested that the bubble size is influenced by the highly subcooled bulk liquid and the bubble size may be limited by the increased thermal non-equilibrium. Decreasing bubble diameter with increasing pressure was also observed by Chen et al. [19]. In the study by Chen et al. [19] the reduced bubble diameter at elevated pressure was said to be physically consistent as the required latent heat to form the same size bubble at higher pressure increases significantly. However, the opposite trend of increasing bubble diameter with increasing pressure was observed by Murshed et al. [20]. The authors give no physical explanation to explain this trend.

A steady decrease in departure diameter with increasing inlet liquid velocity at the elevated pressure condition is shown in Fig. 2. This trend also dominates the low pressure results however there are some cases, particularly at low flow rate, that display a slightly increasing departure diameter with increasing liquid flow rate. Previous studies have reported a decrease in bubble nucleation size with increasing liquid flow rate [7,13,21-26]. Koumoutsos et al. [26] proposes that the decrease in departure size with increasing flow rate is due to a decrease in surface tension force by a thinning of the bubble attachment to the wall. The bubble departure size was observed by Akiyama and Tachibana [24] to decrease linearly with the log of liquid velocity.

The effect of local bulk subcooling on bubble departure diameter is shown by Fig. 3 to decrease significantly with increasing local bulk subcooling for the low pressure data. Other low pressure wall nucleation studies report this same trend in bubble departure diameter [7,23-25,27]. The study of Basu et al. [22] reports a weak trend in bulk liquid subcooling. Interestingly, the bulk liquid subcooling is shown to have very little effect on the bubble departure diameter at the elevated pressure condition. This result may suggest that the bubble departure diameter at low pressure is strongly related to the superheated liquid layer close to the wall where the bubble growth is restricted by the inability to grow into the subcooled bulk fluid. In contrary, at elevated pressure, the independence of bulk subcooling may suggest that the bubble departs before it extends across the superheated layer.

The effect of heat flux on departure diameter is shown in Fig. 4 to have separate trends at the two pressure conditions. At the lower pressure condition the bubble diameter is shown to have an overall decreasing trend with increasing heat flux, while the bubble diameter increases with increasing heat flux at the elevated pressure condition. The data at elevated pressure appears to be much more stable with changes in the wall heat flux than at low pressure where the departure diameter shows large scatter and a much more significant dependence on the wall heat flux. The data of Prodanovic et al. [7] shows this decreasing bubble diameter with increasing heat flux and, much like the present data, a weaker function of heat flux at elevated pressure. An increasing bubble diameter with heat flux has also been shown in literature [13,21]. Basu et al. [22] notes that the bubble diameter increases with increasing wall superheat which also suggests an increase with increasing wall heat flux.

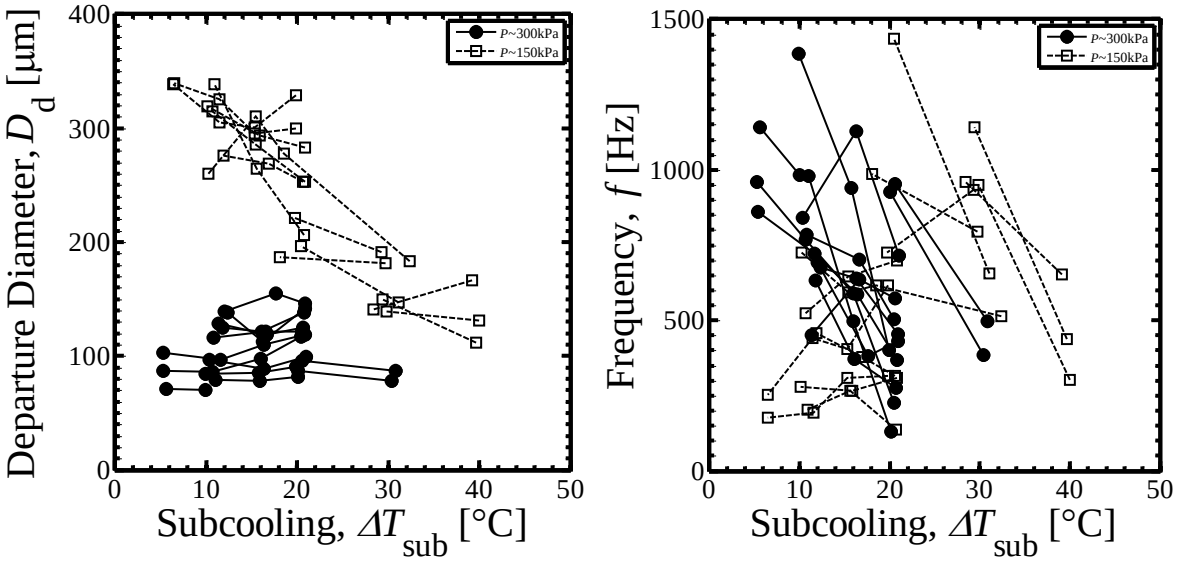

Fig. 3: Effect of local bulk liquid subcooling on bubble departure diameter and frequency

3.2 Bubble Departure Frequency Data

The bubble departure frequency data is also shown in Figs. 2-4. Some cases suggest that the elevated pressure condition tends to increase the departure frequency compared with the lower pressure for data with the same heat flux, subcooling, and inlet liquid velocity. This trend was also reported by Murshed et al. [20]. Increasing system pressure, which has been shown to reduce the bubble departure diameter, suggests that if the growth rate does not change significantly the frequency would increase due to a shorter required growth time [12]. However this rationale is still debatable as Chen et al. [19] reports that the higher required latent heat with increased system pressure should reduce the growth rate. The reduced growth rate and reduced bubble departure size are competing factors affecting the bubble departure frequency.

There is no clear trend in bubble departure frequency with liquid velocity as shown in Fig. 2. There are likely competing effects of velocity on departure frequency. An increase in liquid flow rate decreases growth time by increasing the shearing off of the bubbles from the heater surface. However increasing the velocity also increases the turbulent effects which act to increase the wall temperature drop following a bubble departure. This reduction in wall temperature following bubble departure is expected to increase the bubble wait time [12]. The study of Yin et al. [27] which studied boiling of R134a in a horizontal annular channel, reports a decrease in bubble departure frequency with increase in mass flux. The artificial cavity of Abdelmessih et al. [21] showed no effect due to changes in liquid velocity.

The bubble departure frequency is found to be a strong function of local bulk subcooling which is shown in Fig. 3. The reduction of bubble departure frequency with increased bulk subcooling is expected as lower relative liquid temperature in the bulk fluid will require a longer time to recover the required superheat following a bubble departure [12]. This higher subcooling may also decrease the frequency by increasing the growth time of the nucleating bubbles [25]. The study of Yin et al. [27] also observed this decreasing trend in frequency. Similar to the results presented by Euh et al. [12], this trend is not clear for all cases as some of the low pressure data show an increase with increasing subcooling.

The bubble departure frequency also shows a strong dependence on wall heat flux in Fig. 4 with a large increase in frequency with increasing heat flux. This trend is expected as a larger wall heat flux will produce a larger wall superheat as well as allow for faster recovery of the superheat following bubble departure. The increase in wall superheat directly effects the bubble growth time as the bubble grows due to evaporation at the interface in the superheated liquid region. Furthermore, the faster wall temperature recovery with larger wall heat flux is expected to reduce the wait time between two nucleating bubbles [12,28].

3.3 Bubble Departure Diameter Model Evaluation

The compiled bubble departure diameter database is used to evaluate the current state of departure diameter modeling in Tab. 3 and the three most successful models shown in Fig. 5. Here the mean absolute model error is given as,

$$\text{Mean Absolute Model Error} = \sum \left| \frac{D_{d,Calc} - D_{d,Exp}}{D_{d,Exp}} \right| \quad (2)$$

Modeling difficulty is immediately apparent with orders-of-magnitude error in the current state-of-the-art bubble departure diameter models. The contact angle for the dataset of Yuan et al. [15] was assumed to be 57 degrees based on the similarity of fluid and surface with the present dataset. The bulk liquid temperature,

necessary in the models of Prodanovic et al. [7] and Unal [3], is calculated by the Liu and Winterton [29] model for the dataset of Klausner et al. [13]. The Liu and Winterton [29] model was developed for subcooled boiling and compared with datasets including refrigerants such as R113 used by Klausner et al. [13].

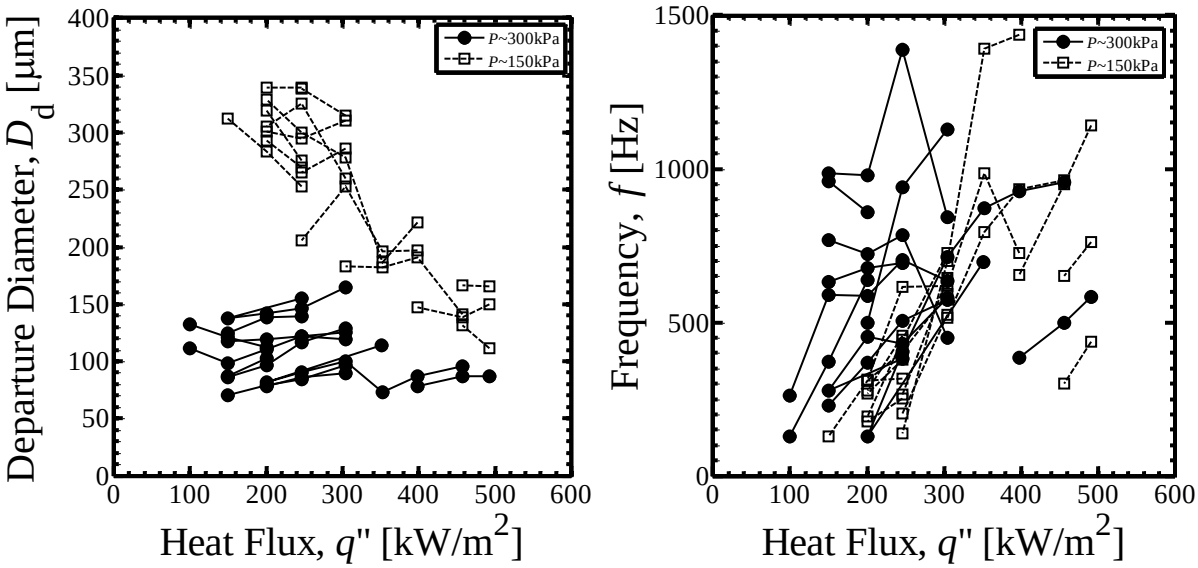

Fig. 4: Effect of wall heat flux on bubble departure diameter and frequency

Over prediction of the departure diameter is shown by the force balance proposed by Fritz [4]. This model was developed by considering surface and buoyancy forces which results in a constant bubble departure diameter for a given fluid and contact angle. The model gives similar prediction accuracy with the refrigerant dataset of Klausner et al. [13] as with water datasets. Kocamustafaogullari and Ishii [5] modified the model of Fritz [4] by proposing dimensionless groups to account for the effect of pressure. The prediction accuracy is significantly improved by this modification and shown in Fig. 5, particularly for the dataset of Yuan et al. [15]. The modification is shown to have a large effect on the refrigerant dataset which is over predicted by Fritz [4] and under predicted by Kocamustafaogullari and Ishii [5]. Similar to these two models, Harada et al. [6] modifies the model by Levy [30] to only consider surface tension and buoyancy as well. In this model the dependence of contact angle is not considered, however marginally better prediction is seen compared with Fritz [4].

The energy balance approach of Unal [3] is shown in Fig. 5 to have mixed prediction capability for the different datasets. The present dataset and the data of Basu [14] shows only small scatter and over prediction with the model, however a lot of scatter is shown in the other two datasets. The refrigerant data of Klausner et al. [13] shows the most scatter which is likely due to invalid application of the heat transfer coefficient and condensation models to refrigerants used in the model development. Scatter in Yuan et al. [15] is likely due to the experimental facility which would have large impact on the energy balance as the heat transfer and local temperature characteristics in this geometry may be much different from the larger channels of the other datasets. From this viewpoint it may be more effective to model the dataset of Yuan et al. [15] with a force balance approach, as seen by the comparison with the model by Kocamustafaogullari and Ishii [5], than a local energy balance approach.

The model by Prodanovic et al. [7] for the maximum bubble size is purely empirical and shows the best overall agreement with the bubble departure database. The low pressure dataset of the present study and the data of Basu [14] shows particularly good agreement with only a slight over prediction. Some scatter is seen in the elevated pressure data of the present study however this data is also predicted most accurately by Prodanovic et al. [7]. The model under predicts the large nucleating bubbles of Yuan et al. [15] dataset. The model has difficulty with the refrigerant data of Klausner et al. [13] likely due to its empirical nature. The recent force balance model of Situ et al. [11] predicts very large bubble departure diameter for the present dataset and the dataset of Basu [14]. This is due to the large growth force at high wall superheat which holds the bubble on the wall, compared with the drag force which acts to remove the bubble from the nucleation site. It should be noted that this model by Situ et al. [11] was published without benchmark with experimental data.

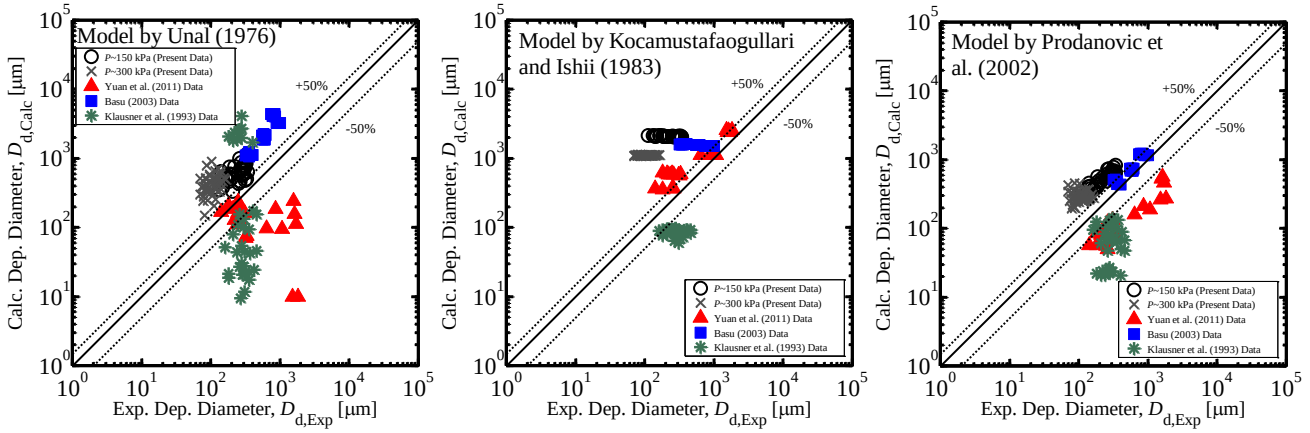

Fig. 5: Comparison of available bubble departure diameter models with the available bubble departure diameter database

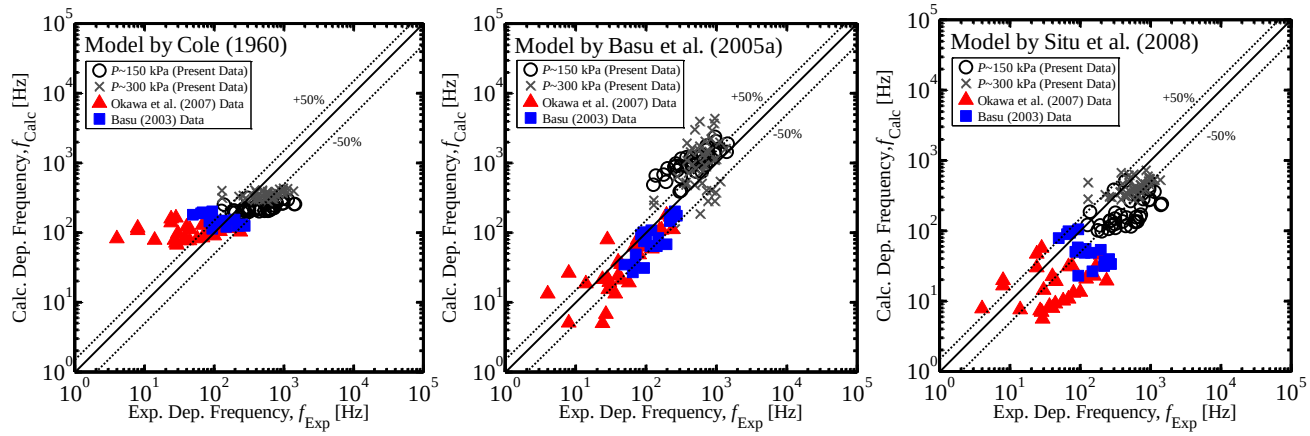

Fig. 6: Comparison of available bubble departure frequency models with the available bubble departure frequency database

3.4 Bubble Departure Frequency Model Evaluation

Select bubble departure frequency models described previously are compared with the available database in Tab. 4 and the most successful models shown in Fig. 6. To isolate the prediction of departure frequency the measured departure diameter data is used in the model calculations. Interestingly, the model by Cole [9] which is based on horizontal pool boiling, shows relatively good agreement with database. The frequency prediction breaks down at the very low frequencies of Okawa et al. [16] however good prediction is shown for the current dataset and the dataset of Basu [14]. The model by Cole [9] shown in Tab. 1 only varies with pressure and departure diameter for a given working fluid.

A lot of scatter is shown in the model of Podowski et al. [8]. Error of several orders of magnitude is shown in the low pressure data however very good prediction is shown at the elevated pressure condition. The disparity in accuracy between the low and elevated pressure condition suggests the differences in driving mechanism with changing pressure. Little scatter is shown by the model of Basu et al. [22] at low pressure. The data of Basu [14], and much of the Okawa et al. [16] data, is slightly under-predicted while the data of the present study is largely over-predicted.

Table 3. Departure diameter model benchmark with database

Model	Mean Absolute Model Error [%]				
	Klausner et al. [13]	Basu [14]	Yuan et al. [15]	Present Study	
				150 kPa	300 kPa
Fritz [4]	214.6	208.9	809.4	1332.4	2910.2
Unal [3]	274.9	289.0	56.5	167.8	327.0
Kocamustafaogullari and Ishii [5]	68.3	183.0	93.9	839.1	989.3
Prodanovic et al. [7]	74.6	33.2	69.4	131.3	192.2
Situ et al. [11]	NA	430.5	59.1	1181.1	543.8
Harada et al. [6]	143.7	224.1	401.7	691.0	1561.7

Table 4. Departure frequency model benchmark with database

Model	Mean Absolute Model Error [%]*			
	Basu [14]	Okawa et al. [16]	Present Study	
			150 kPa	300 kPa
Cole [9]	77.6	299.1	49.7	49.0
Podowski et al. [8]	288.0	1031.6	164.2	41.4
Basu et al. [10]	33.9	55.8	133.4	126.5
Situ et al. [11]	60.4	78.1	58.4	43.8

Euh et al. [12]	47.6	79.8	58.8	67.3
*Assuming the accurate closure of bubble departure diameter (experimental value)				

The semi-empirical model by Situ et al. [11] is shown in Fig. 6 to give consistent agreement over the available data. The accuracy of the data at elevated pressure speaks to the effectiveness of defining proper dimensionless groups. The empirical constants were determined without an elevated pressure dataset yet the prediction is consistent with the accuracy of the low pressure data. This result advocates for the proposed non-dimensional group based on the nucleate boiling heat flux as shown in Tab. 1 The recent work of Euh et al. [12], which modified the empirical constants of Situ et al. [11], shows less scatter in the model benchmark however has more error at elevated pressure which it was reportedly modified to incorporate.

The dependence of bubble departure diameter on the frequency models is important to note. Considering the large errors in the current bubble departure diameter models shown in Fig. 2 and summarized in Tab. 3, the accuracy of the bubble departure frequency will be greatly deteriorated by the departure diameter if a calculated value was used. Given the difficulty to predict the bubble departure diameter, the most appropriate bubble departure frequency model may be the model which is the weakest function of departure diameter.

4 Conclusions

A complete review of common bubble departure diameter and bubble departure frequency models is compared against available data in literature as well as a new dataset. The new data set covers a wider range of flow conditions in a vertical, internally heated, annulus channel and allows for investigation of system conditions on the trends in departure diameter and frequency. From the analysis of the new dataset and the model comparison with the compiled database the following conclusions should be considered,

- The departure diameter is shown to be a strong function of liquid subcooling and wall heat flux at low pressures, and bulk liquid flow rate at elevated pressures.
- The departure frequency is shown to be a strong function of liquid subcooling and wall heat flux.
- Bubble departure frequency has been modeled with reasonable accuracy over the range of conditions considered given accurate closure of bubble departure diameter.
- The current bubble departure diameter modeling shows significant inaccuracies and scatter in the experimental data.

Future work on this topic should include a new modeling study of the bubble departure diameter in order to properly consider wall nucleation effects in flow boiling.

Acknowledgments

This material is based upon work supported under a Department of Energy Nuclear Energy University Program Graduate Fellowship.

References

[1] Hibiki, T., and Ishii, M. 2003. “Active nucleation site density in boiling systems”. *Int. J. Heat Mass Trans.*, 46, pp. 2587–2601. DOI:10.1016/S0017-9310(03)00031-0

[2] Hibiki, T., and Ishii, M. 2009. “Interfacial area transport equations for gas-liquid flow”. *J. Comp. Multiphase Flows*, 1 (1), pp. 1–22. DOI:10.1260/175748209787387089

[3] Unal, H. C. 1976. “Maximum bubble diameter, maximum bubble growth time and bubble growth rate during subcooled nucleate flow boiling of water up to 17.7mn-m2”. *Int. J. Heat Mass Trans.*, 19 (6), pp. 643–649.

[4] Fritz, W. 1935. “The calculation of the maximiun volume of steam bladders”. *Physikalische Zeitschrift* , 36 , pp. 379–384.

[5] Kocamustafaogullari, G., and Ishii, M. 1983. “Interfacial area and nucleation site density in boiling systems”. *Int. J. Heat Mass Trans.*, 26 (9), pp. 1377–1387.

[6] Harada, T., Nagakura, H., and Okawa, T. 2010. “Dependence of bubble behavior in subcooled boiling on surface wettability”. *Nucl. Eng. Des*., 240 (12), pp. 3949–3955.

[7] Prodanovic, V., Fraser, D., and Salcudean, M. 2002. “Bubble behavior in subcooled flow boiling of water at low pressures and low flow rates”. *Int. J. Multiphase Flow*, 28 (1), pp. 1–19. DOI:10.1016/S0301-9322(01)00058-1

[8] Podowski, R., Drew, D., Lahey, J., R.T., and Podowski, M. 1997. A mechanistic model of the ebullition cycle in forced convection subcooled boiling. NURETH 8. Kyoto, Japan.

[9] Cole, R. 1960. “A photographic study of pool boiling in the region of the critical heat flux”. *Aiche J.*, 6 (4), pp. 533–538.

[10] Basu, N., Warrier, G. R., and Dhir, V. K. 2005. “Wall heat flux partitioning during subcooled flow boiling: Part 1 - model development”. *J. Heat Trans.*, 127 (2), pp. 131–140.

[11] Situ, R., Ishii, M., Hibiki, T., Tu, J. Y., Yeoh, G. H., and Mori, M. 2008. “Bubble departure frequency in forced convective subcooled boiling flow”. *Int. J. Heat Mass Trans.*, 51 (25–26), pp. 6268–6282.

[12] Euh, D., Ozar, B., Hibiki, T., Ishii, M., and Song, C.-H. 2010. “Characteristics of bubble departure frequency in a low-pressure subcooled boiling flow”. *J. Nucl. Sci. Tech*., 47 (7), pp. 608–617. DOI:10.1080/18811248.2010.9720958

[13] Klausner, J. F., Mei, R., Bernhard, D. M., and Zeng, L. Z. 1993. “Vapor bubble departure in forced-convection boiling”. *Int. J. Heat Mass Trans.*, 36 (3), pp. 651–662.

[14] Basu, N. 2003. “Modeling and experiments for wall heat flux partitioning during subcooled flow boiling of water at low pressures”. PhD thesis, University of California, Los Angeles, CA.

[15] Yuan, D. W., Pan, L. M., Chen, D. Q., Zhang, H., Wei, J. H., and Huang, Y. P. 2011. "Bubble behavior of high subcooling flow boiling at different system pressure in vertical narrow channel". *Applied Thermal Eng*., 31 (16), pp. 3512–3520.

[16] Okawa, T., Kubota, H., and Ishida, T. 2007. "Simultaneous measurement of void fraction and fundamental bubble parameters in subcooled flow boiling". *Nucl. Eng. Des*., 237 (10), pp. 1016–1024. DOI:10.1016/j.nucengdes.2006.12.010

[17] Martinez-Cuenca, M., Brooks, C.S., Julia, E., Hibiki, T., Ishii, M. 2015. "Stochastic Nature of Wall Nucleation and Its Impact on the Time Average Boundary Condition". *J. Heat Transfer*, 137, DOI: 10.1115/1.4028975.

[18] Ozar, B., Brooks, C.S., Hibiki, T., and Ishii, M. 2013. "Interfacial area transport of vertical steam-water two-phase flow in an annulus channel at elevated pressures". *Int. J. Heat Mass Trans*., 57, pp. 504–518. DOI: 10.1016/j.ijheatmasstransfer.2012.10.059

[19] Chen, D., Pan, L., Yuan, D., Zhang, H., Xu, J., and Huang, Y. 2011. "The nature of bubble growth under different system pressures in a narrow channel". *Nucl. Eng. Des*., 241 (3), pp. 785–791. DOI: 10.1016/j.nucengdes.2010.12.013

[20] Murshed, S. M. S., Vereen, K., Strayer, D., and Kumar, R. 2010. "An experimental investigation of bubble nucleation of a refrigerant in pressurized boiling flows". *Energy*, 35 (12), pp. 5143–5150. DOI: 10.1016/j.energy.2010.07.052

[21] Abdelmessih, A., Hooper, F. C., and Nangia, S. 1972. "Flow effects on bubble growth and collapse in surface boiling". *Int. J. Heat Mass Trans*., 15 (1), pp. 115–124.

[22] Basu, N., Warrier, G. R., and Dhir, V. K. 2005. "Wall heat flux partitioning during subcooled flow boiling: Part ii - model validation". *J. Heat Trans*., 127 (2), pp. 141–148.

[23] McAdams, W. H., Kennel, W. E., Minden, C. S., Carl, R., Picornell, P. M., and Dew, J. E. 1949. "Heat transfer at high rates to water with surface boiling". *Ind. Eng. Chem*., 41 (9), pp. 1945–1953. DOI:10.1021/ie50477a027

[24] Akiyama, M., and Tachibana, F. 1974. "Motion of vapor bubbles in subcooled heated channel". *Bulletin JSME*, 17 (104), pp. 241–247. DOI: 10.1299/jsme1958.17.241

[25] Maity, S. 2000. "Effect of velocity and gravity on bubble dynamics". PhD thesis, University of California, Los Angeles, CA.

[26] Koumoutsos, N., Moissis, R., and Spyridonos, A. 1968. "A study of bubble departure in forced-convection boiling". *J. Heat Trans*., pp. 223–229. DOI: 10.1115/1.3597483

[27] Yin, C. P., Yan, Y. Y., Lin, T. F., and Yang, B. C. 2000. "Subcooled flow boiling heat transfer of r-134a and bubble characteristics in a horizontal annular duct". *Int. J. Heat Mass Trans*., 43 (11), pp. 1885–1896.

[28] Thorncroft, G. E., Klausner, J. F., and Mei, R. 1998. "An experimental investigation of bubble growth and detachment in vertical upflow and downflow boiling". *Int. J. Heat Mass Trans*., 41 (23), pp. 3857–3871.

[29] Liu, Z., and Winterton, R. H. S. 1991. "A general correlation for saturated and subcooled flow boiling in tubes and annuli, based on a nucleate pool boiling equation". *Int. J. Heat Mass Trans*., 34 (11), pp. 2759–2766.

[30] Levy, S. 1967. "Forced convection subcooled boiling - prediction of vapor volumetric fraction". *Int. J. Heat Mass Trans*., 10 (7), pp. 951–964. DOI: 10.1016/0017-9310(67)90071-3

Appendix A: Tabulated dataset

The experimental dataset taken in the internally heat annulus channel discussed in section 2 and presented in detail in section 3 is tabulated here.

Table 5. New experimental dataset for bubble departure diameter and frequency

Run	$j_{f,in}$ [m/s]	q'' [kW/m^2]	P [kPa]	ΔT_{sub} [^{o}C]	D_d [mm]	f [Hz]
1	1.00	304	301	21.1	9.97E-02	7.14E+02
2	1.01	246	301	20.0	9.07E-02	4.03E+02
3	0.997	200	301	20.2	8.14E-02	1.29E+02
4	1.00	351	301	19.9	1.14E-01	6.97E+02
5	1.01	200	302	16.0	7.77E-02	4.98E+02
6	1.01	246	302	15.9	8.57E-02	9.39E+02
7	1.00	304	302	16.4	8.92E-02	1.13E+03
8	1.01	304	303	10.4	9.65E-02	8.42E+02
9	0.990	246	303	10.0	8.39E-02	1.39E+03
10	0.987	200	301	11.1	7.92E-02	9.79E+02
11	0.995	150	301	10.1	6.99E-02	9.85E+02
12	1.02	150	304	5.70	7.07E-02	1.14E+03
13	0.513	304	300	20.7	1.25E-01	5.73E+02
14	0.508	246	301	20.6	1.21E-01	5.04E+02
15	0.503	200	301	21.0	1.19E-01	3.69E+02
16	0.509	150	300	20.5	1.17E-01	2.28E+02
17	0.501	304	301	16.8	1.19E-01	6.36E+02
18	0.510	246	302	16.7	1.21E-01	7.02E+02
19	0.511	200	302	16.5	1.10E-01	5.85E+02
20	0.509	150	302	16.1	9.79E-02	5.89E+02
21	0.508	100	301	15.0	1.11E-01	2.63E+02
22	0.490	304	304	11.4	1.29E-01	4.51E+02

23	0.500	246	301	10.9	1.16E-01	7.83E+02
24	0.499	200	303	11.7	9.67E-02	7.22E+02
25	0.489	150	303	10.8	8.61E-02	7.67E+02
26	0.509	200	300	5.50	1.03E-01	8.59E+02
27	0.503	150	300	5.40	8.72E-02	9.60E+02
28	0.247	304	303	22.5	1.64E-01	5.78E+02
29	0.256	246	303	21.0	1.46E-01	4.32E+02
30	0.259	200	302	21.0	1.42E-01	4.54E+02
31	0.259	150	302	20.8	1.38E-01	2.77E+02
32	0.247	246	302	17.8	1.55E-01	3.83E+02
33	0.253	200	303	16.4	1.12E-01	6.39E+02
34	0.256	150	301	16.2	1.21E-01	3.72E+02
35	0.254	100	301	16.4	1.33E-01	1.30E+02
36	0.250	246	301	12.1	1.39E-01	6.93E+02
37	0.246	200	301	12.4	1.38E-01	6.76E+02
38	0.257	150	302	11.9	1.25E-01	6.32E+02
39	1.01	304	151	20.6	2.53E-01	7.00E+02
40	0.994	246	152	20.5	2.06E-01	1.38E+02
41	0.996	304	152	15.2	2.86E-01	6.46E+02
42	1.00	246	152	15.4	2.65E-01	2.64E+02
43	1.03	304	153	10.5	3.15E-01	5.25E+02
44	0.999	246	152	10.7	3.38E-01	2.03E+02
45	0.504	304	153	18.3	2.78E-01	6.18E+02
46	0.503	246	153	19.7	3.00E-01	6.16E+02
47	0.501	200	151	19.6	3.28E-01	3.15E+02
48	0.493	304	150	15.2	3.10E-01	5.93E+02
49	0.502	246	152	15.1	2.95E-01	4.04E+02
50	0.500	200	152	15.1	3.01E-01	3.09E+02
51	0.494	304	151	10.0	2.60E-01	7.25E+02
52	0.502	246	151	11.3	3.25E-01	4.42E+02
53	0.508	200	153	11.3	3.05E-01	1.92E+02
54	0.503	246	151	6.30	3.40E-01	2.53E+02
55	0.507	200	152	6.20	3.39E-01	1.77E+02
56	0.254	246	154	20.4	2.53E-01	3.16E+02
57	0.248	200	154	20.7	2.83E-01	3.10E+02
58	0.244	150	153	21.5	3.12E-01	1.27E+02
59	0.250	246	151	16.6	2.69E-01	3.78E+02
60	0.253	200	151	15.6	2.93E-01	2.67E+02
61	0.250	246	153	11.7	2.76E-01	4.56E+02
62	0.254	200	152	9.90	3.19E-01	2.79E+02
63	1.01	492	152	39.4	1.12E-01	4.37E+02
64	0.998	457	152	39.8	1.31E-01	3.01E+02
65	1.03	492	153	29.2	1.49E-01	1.14E+03
66	1.02	457	154	29.6	1.39E-01	9.49E+02
67	1.02	398	154	30.9	1.47E-01	6.55E+02
68	0.993	398	154	20.2	1.97E-01	1.44E+03
69	1.01	352	153	20.4	1.96E-01	1.39E+03
70	0.496	492	152	39.5	1.65E-01	7.61E+02
71	0.500	457	153	38.9	1.67E-01	6.52E+02
72	0.497	457	154	28.2	1.41E-01	9.61E+02
73	0.500	398	153	29.0	1.91E-01	9.33E+02
74	0.505	352	153	29.5	1.82E-01	7.93E+02
75	0.505	304	153	32.2	1.83E-01	5.15E+02
76	0.498	398	154	19.5	2.21E-01	7.26E+02
77	0.508	352	153	17.9	1.87E-01	9.85E+02
78	1.01	492	302	30.8	8.65E-02	5.82E+02
79	1.02	457	302	30.9	8.66E-02	4.99E+02
80	1.02	398	302	30.4	7.84E-02	3.85E+02
81	1.02	457	301	20.6	9.55E-02	9.55E+02
82	1.03	398	302	20.2	8.72E-02	9.27E+02
83	1.02	352	302	20.2	7.32E-02	8.73E+02

Table captions:

Figure captions: